Neurobiology of Disease 95 (2016) 134–144

Contents lists available at ScienceDirect

Neurobiology of Disease

journal homepage: www.elsevier.com/locate/ynbdi

# Minute amounts of hamartin wildtype rescue the emergence of tuber-like lesions in conditional *Tsc1* ablated mice

Barbara K. Robens [a], Alexander Grote [b], Julika Pitsch [a], Susanne Schoch [a], Carlos Cardoso [c,d,1], Albert J. Becker [a,*,1]

[a] Section for Translational Epilepsy Research, Dept. of Neuropathology, Germany
[b] Neurosurgery, Bonn Univ. Clinic, Germany
[c] INSERM, Institut de Neurobiologie de la Méditerranée, Marseille, France
[d] Aix-Marseille University, UMR 901 Marseille, France

ARTICLE INFO

*Article history:*
Received 15 March 2016
Revised 5 July 2016
Accepted 13 July 2016
Available online 15 July 2016

*Keywords:*
*TSC1*
Tuberous sclerosis
Focal cortical dysplasia
Mammalian target of rapamycin
Cortical tuber
*In utero* electroporation

ABSTRACT

Tuberous sclerosis (TSC) is a phacomatosis associated with highly differentiated malformations including tubers in the brain. Those are composed of large dysplastic neurons and 'giant cells'. Cortical tubers are frequent causes of chronic seizures and resemble neuropathologically focal cortical dysplasias (FCD) type IIb. Patients with $FCD_{IIb}$, however, lack additional stigmata of TSC. Mutations and allelic variants of the *TSC1* gene have been observed in patients with tubers as well as $FCD_{IIb}$. Those include hamartin$^{R692X}$ and hamartin$^{R786X}$, stop mutants frequent in TSC patients and hamartin$^{H732Y}$ frequent in $FCD_{IIb}$. Expression of these variants in cell culture led to aberrant distribution of corresponding proteins. We here scrutinized morphological and structural effects of these *TSC1* variants by intraventricular *in utero* electroporation (IUE), genetically mimicking the discrete focal character and a somatic postzygotic mosaicism of the lesion, focusing on the gene dosage required for tuber-like lesions to emerge in *Tsc1*$^{flox/flox}$ mice. Expression of only hamartin$^{R692X}$ as well as hamartin$^{R786X}$ led to a 2-fold enlargement of neurons with high pS6 immunoreactivity, stressing their *in vivo* pathogenic potential. Co-electroporation of the different aberrant alleles and varying amounts of wildtype *TSC1* surprisingly revealed already minimal amounts of functional hamartin to be sufficient for phenotype rescue. This result strongly calls for further studies to unravel new mechanisms for substantial silencing of the second allele in cortical tubers, as proposed by Knudson's '2-hit hypothesis'. The rescuing effects may provide a promising basis for gene therapies aiming at reconstituting hamartin expression in tubers.



## 1. Introduction

Tuberous sclerosis (TSC) is an autosomal-dominant inherited multi organic disorder affecting approximately 1/6000 individuals (Hengstschläger et al., 2001). This phacomatosis is characterized by benign tumors and dysplastic lesions in many organs including skin, kidney, lungs, heart and brain (Gomez, 1988). In the latter, cortical tubers composed of large, dysmorphic neurons and so-called giant cells are frequently associated with pharmacoresistant epilepsy. Cortical dysplasias, associated with focal epilepsies and composed of dysplastic cytomegalic neurons and so-called balloon cells ($FCD_{IIb}$ (Blümcke et al., 2010)), are histomorphologically virtually indistinguishable from cortical tubers, although the patients generally lack additional features of a neurocutaneous phacomatosis (Taylor et al., 1971).

TSC is commonly caused by mutations in either *TSC1* on chromosome 9q34 (Van Slegtenhorst et al., 1997) or *TSC2* on chromosome 16p13.3 (Carbonara et al., 1994; Sampson and Harris, 1994). Hamartin and tuberin, the corresponding gene products, form a heteromer with a central role as tumor suppressor in the phosphatidylinositol 3-kinase (Pi3K) pathway (Baybis et al., 2004; Van Slegtenhorst et al., 1997, 1998, 1999). Extracerebral neoplasms frequently have a parallel loss of heterozygosity (LOH) (Green et al., 1994). LOH, however, has been rarely detected in TSC brain lesions (Henske et al., 1996). Further evidence suggests that somatic second-hit events in *TSC1* heterozygous individuals may account for cortical tubers (Chan et al., 2004; Crino et al., 2010; Henske et al., 1997), and in fact no tubers have been reported in mice heterozygous for *Tsc1* (Piedimonte et al., 2006; Scheidenhelm and Gutmann, 2004; Uhlmann et al., 2002). However, another study reported second hit mutations to be rare events in cortical tubers (Qin et al., 2010). Furthermore, the TSC pathway in neurons was proposed to be highly sensitive to gene dosage effects as *Tsc1* haploinsufficiency for example impairs neuronal morphology (Tavazoie et al., 2005).

We have recently shown that the expression of hamartin$^{R692X}$ as well as hamartin$^{R786X}$, two stop mutants frequently found in TSC patients

* Corresponding author at: Department of Neuropathology, University of Bonn Medical Center, Sigmund-Freud Str. 25, D-53127 Bonn, Germany.
*E-mail address:* albert_becker@uni-bonn.de (A.J. Becker).
[1] These authors contributed equally to the work.
**Available online on ScienceDirect (www.sciencedirect.com).**

http://dx.doi.org/10.1016/j.nbd.2016.07.006
0969-9961/

(Dabora et al., 2001; Hung et al., 2006; Van Slegtenhorst et al., 1999) results in substantial binding deficits with tuberin and aberrant distribution of the mutated hamartin *in vitro* (Lugnier et al., 2009). In addition, expression of an allelic polymorphism significantly increased in $FCD_{IIb}$ patients, a base exchange from C to G in exon 17 of *TSC1* at nucleotide 2415 resulting in a switch from histidine to tyrosine at codon 732 (hamartin$^{H732Y}$) (Becker et al., 2002), leads to impaired TSC1-TSC2 heteromer formation and aberrant subcellular distribution of the hamartin$^{H732Y}$ (Lugnier et al., 2009).

Based on these observations, we here aimed to elucidate the morphological and structural effects of respective *TSC1* variants *in vivo* with a particular emphasis on the question which gene dosage is required for a morphological phenotype reflecting tuber-like lesions to emerge.

## 2. Materials and methods

### 2.1. Study approval

All experiments were performed in accordance with the guidelines of the European Union and the University of Bonn Medical Center Animal Care Committee.

### 2.2. Intraventricular in utero electroporation in mice

The C57Bl/6 Tsc1tm1Djk/J (C57BL/6N-*Tsc1*$^{flox/flox}$) mice strain provided by The Jackson Laboratory (JAX) is an established mouse model for Cre mediated *Tsc1* knockout and thus for investigating tuberous sclerosis (Feliciano et al., 2011). For *in utero* electroporation (IUE) we backcrossed C57Bl/6N-*Tsc1*$^{flox/flox}$ mice from the C57Bl/6 background to the CD1 (JAX) background for three generations. For accelerated backcrossing, the genome of the F2 and F3 generation was genotyped for C57Bl/6 specific SNPs. Mice with lowest C57BL/6 SNP-score and homozygous for *Tsc1*-flox were used for further breeding. The *Tsc1*$^{flox/flox}$ mouse strain used in the present study has a mixed genetic background. We will refer to it as 'CD1-*Tsc1*$^{flox/flox}$' mice, since the CD1 background is predominant due to the fact that SNP sequencing after the third generation estimated 90% CD1 and 10% C57Bl/6 genetic content.

CD1-*Tsc1*$^{flox/flox}$ females were crossed with CD1-*Tsc1*$^{flox/flox}$ males for validation of the new strain or with C57BL/6-*Tsc1*$^{flox/flox}$ males for all other experiments because of increased IUE efficiency compared to CD1 × CD1 breedings. The IUE was performed as described recently (Grote et al., 2016). Shortly, pregnant mice (E14, E16, E17 or E18) were anesthetized with isoflurane and injected with Gabrilen (5 mg/kg) and Buprenovet (0.05 mg/kg) 30 min prior to the IUE as analgesia. After exposure of the uterine horns each embryo was injected once with 0.5–1 μl DNA (with a concentration of 3.0–5.0 μg/μl) and fast green (1 mg/ml, Sigma, St. Louis) with a pulled and beveled glass capillary (Drummond Scientific, PA) and a microinjector (Picospritzer III, General Valve Corporation, USA) into one lateral ventricle. By administering five electric pulses charged to 45 V electroporation was conducted. A 7 mm electrode was placed to target cortical ventricular and subventricular progenitors in the somatosensory and motor cortex (Saito, 2006). Successfully electroporated mice were anesthetized with ketamine/xylazine (100 mg/kg and 10 mg/kg, respectively) three to four weeks after birth and sacrificed trough cardiac 4% PFA perfusion for further analysis.

### 2.3. Generation of constructs

Expression fragments for human *TSC1*-WT, *TSC1*-H732Y, *TSC1*-R786X, *TSC1*-R692X and Cre-recombinase were amplified by Polymerase Chain reaction with specific primers (Table 1) and ligated into the pB-CAG-2A-mCherry or pB-CAG-GFP vector (kindly provided by Joe LoTurco; University of Connecticut) *via* KpnI and AgeI or EcoRI and XmaI restriction sites. Table 1 gives an overview of all used primers and restriction enzyme recognition sequences (small letters).

**Table 1**
Plasmid generation.

| Plasmid | | 5′–3′ sequence |
|---|---|---|
| CAG-Cre-GFP | fw | GCGgaattcATGTCCAATTTACTGACCGTACA |
| CAG-Cre-GFP | rev | GCGcccgggcATCGCCATCTTCCAGCAGG |
| *TSC1*-WT-2A-mCherry | fw | GCGggtaccATGGCCCAACAAGCAAATGTC |
| *TSC1*-WT-2A-mCherry | rev | GCGaccggtGCTGTGTTCATGATGAGTCTCA |
| *TSC1*-H732Y-2A-mCherry | fw | GCGggtaccATGGCCCAACAAGCAAATGTC |
| *TSC1*-H732Y-2A-mCherry | rev | GCGaccggtGCTGTGTTCATGATGAGTCTCA |
| *TSC1*-R786X-2A-mCherry | fw | GCGggtaccATGGCCCAACAAGCAAATGTC |
| *TSC1*-R786X-2A-mCherry | rev | GCGaccggtGTCATGCTGCAGCTGTCTGA |
| *TSC1*-R692X-2A-mCherry | fw | GCGggtaccATGGCCCAACAAGCAAATGTC |
| *TSC1*-R692X-2A-mCherry | rev | GCGaccggtGAGGGTGCGGATCTCATCT |

### 2.4. Immunohistochemistry

For co-immunofluorescence stainings, brains from P23-30, electroporated and PFA-perfused mice were collected and cut to 80 μm slices on a Microm HM 650V vibratome (Thermo Scientific, MA). Afterwards, brain slices were washed in 0.1% Triton X-100 PBS solution and blocked with 0.1% Triton X-100, 0.1% Tween 20, 4% bovine serum albumin (BSA) in pH 7.7 TBS for 1 h. This was followed by an overnight incubation with primary antibodies against mouse anti-NeuN (1:400 - Millipore, MA; Antibody Registry: AB_331679 and AB_2298772), Phospho-S6 Ribosomal Protein (Ser235/236) #2211 or (Ser240/244) #2215 (1:500 - Cell Signaling, MA; Antibody Registry: AB_331679 and AB_331682) at 4 °C (both antibodies had similar staining patterns). After three washing steps, brains were incubated with secondary fluorescently labeled antibodies Alexa Fluor® 647 and 405 (1:200 - Life Technologies, NY) for 1 h and mounted on glass plates with vectashield (Vector Laboratories, CA).

### 2.5. Image analysis and quantification

Z-stack maximum intensity projection confocal images were taken from 80 μm mouse brains after intraventricular *in utero* electroporation with a Nikon Eclipse Ti confocal microscope (Nikon Instruments, Germany) and analyzed for different parameters.

First, neurons form brain slices immunolabeled with antibodies against NeuN and Phospho-S6 Ribosomal Protein Ser240/244 (further referred to as pS6) were analyzed with respect to their pS6 fluorescence intensity and their mean soma size. mCherry-labeled neurons were automatically recognized by the region of interest (ROI) auto-detect function of the NIS elements analysis software (Nikon Instruments, Germany) and parameters such as cell size and fluorescence intensity were generated for each individual ROI. For each brain slice analyzed, all cells that were bright enough to be recognized by the software were included in the analysis.

Final positioning of cortical neurons was analyzed by defining the borders of the six-layered cortex by NeuN staining and the percentage of all electroporated neurons in each layer was calculated. Additionally, the mean distribution of electroporated cells all over the cortex was analyzed by measuring the distance (in μm) of each individual electroporated cell to the upper border of layer I. The mean for each developmental time point was summarized for control and Cre-electroporated *Tsc1* knockout neurons.

Next, confocal maximum intensity projection images of single *in utero* electroporated cortical neurons were subjected to morphometric analyses and quantification using ImageJ software (Wayne Rasband, Maryland). For Sholl analysis each branch from mCherry-labeled *in utero* electroporated neurons was traced from branching point to the tip. On each traced image rings with 10 μm intervals were overlaid and the numbers of neurite intersections were counted for each circle (Ristanović et al., 2006; Sholl, 1953).

### 2.6. Statistical analyses

Different statistical tests were used: Kolmogorov-Smirnov test was used for Sholl analysis. Chi-square test and Two-way ANOVA with Bonferroni post-correction were used for assessing the amount of neurons in different cortical layers. In addition, to verify this approach the neuronal distance-distributions within the cortex were assessed with Mann-Whitney *U* test. One-way ANOVA with Bonferroni post-correction was carried out for cell size and pS6 fluorescence intensity quantification. For all analyses, neurons from all animals in each group were aggregated for statistical comparison, except for the Chi-square test; here the mean values from each group were compared. All error bars are indicated as the 'standard error of the mean' (SEM).

## 3. Results

### 3.1. Single cell Cre expression in CD1-*Tsc1*$^{flox/flox}$ mice leads to increased mTOR pathway activation and dysplastic brain lesions

To knockout *Tsc1* in a restricted focal cortical area in a subset of precursor cells during mid-corticogenesis and to investigate the resulting lesion, we *in utero* electroporated *Tsc1*$^{flox/flox}$ mice with a Cre-recombinase (Cre) expressing plasmid at E14. Litter survival after IUE is substantially higher in CD1 mice in comparison to the commonly used laboratory C57BL/6 strain due to very poor mothering instincts of the latter (Baumgart and Grebe, 2015; Cobolli Gigli et al., 2016; and our observations). In an attempt to address this problem, we generated *Tsc1*$^{flox/flox}$ mice in the CD1 background (CD1-*Tsc1*$^{flox/flox}$ mice). A successful allele-of-interest transfer from the C57Bl/6 background to CD1 was recently published and used for an improved Rett syndrome mouse model for similar reasons (Cobolli Gigli et al., 2016). We first validated that also in this genetic background Cre-mediated deletion of *Tsc1* results in an activation of the mTOR pathway by analyzing the level of pS6 immunoreactivity (IR) and cell volume/soma size at P24-30. An increase in these parameters has been reported after *Tsc1* knockout in the C57Bl/6 background (Feliciano et al., 2011). In accordance, we observed strong pS6 immunolabeling only in the ipsilateral cortex of *Tsc1*$^{flox/flox}$ mice *in utero* electroporated with CAG-Cre-GFP together with mCherry as a volume dye (Fig. 1A, C, right panel) but not in the contralateral side (Fig. 1B, right panel) or after electroporation of mCherry alone (Fig. 1D, right panel) (mCherry/*Tsc1*$^{flox/flox}$ 483.2 a.u. ± 10.6 *vs.* mCherry/Cre$^{+}$/*Tsc1*$^{-/-}$ 1339.5 a.u. ± 39.1; One-way ANOVA with Bonferroni post-correction ***$p < 0.001$, N = 7–8 mice with 23–30 cells each). Analysis of individual neurons also revealed an increase in soma size in Cre-positive *Tsc1* ablated neurons (Fig. 1C) compared to neurons only electroporated with mCherry (Fig. 1D) (mCherry/*Tsc1*-$^{flox/flox}$ 163.7 μm$^2$ ± 3.0 *vs.* mCherry/Cre$^{+}$/*Tsc1*$^{-/-}$ 391.9 μm$^2$ ± 5.3; One-way ANOVA with Bonferroni post-correction ***$p < 0.001$, N = 7–8 mice with 41–60 neurons each). Previous studies showed that hyperactivation of the mTOR pathway in neurons leads to an excessive branching and a thickening of the apical dendrite (Crino et al., 2010; Feliciano et al., 2013). Sholl analysis of single neurons of CD1-*Tsc1*$^{flox/flox}$ mice electroporated with CAG-Cre-GFP showed an aberrantly increased dendrite complexity in the absence of *Tsc1* (Fig. 1E, F) in contrast to control electroporated neurons (Fig. 1E, G). Furthermore, Cre-induced *Tsc1* knockout resulted in an increased axon diameter (Fig. 1H, I). Together, these results demonstrate that Cre-mediated ablation of *Tsc1* in the CD1 background causes phenotypically identical changes as previously observed in the C57Bl/6 background indicating the functionality of this mouse line for further studies.

### 3.2. Tsc1 knockout at different points of embryonic development results in similar neuropathological alterations

Next we examined if the time point of hamartin ablation during embryonic development impacts the observed neuropathological alterations. To this end we performed IUE of CAG-Cre-GFP/mCherry or mCherry alone at E16 to E18. As knockout of *Tsc1* at E14 had resulted in a substantially increased soma size, we quantified this parameter as an indicator for mTOR pathway up-regulation due to *Tsc1* loss. This quantification revealed an approx. 2-fold enlargement of soma size at P24-30 after Cre-induced *Tsc1* knockout both at E16 and at E17 (Fig. 2A-C) (E16: mCherry/*Tsc1*$^{flox/flox}$ 153.2 μm$^2$ ± 4.2 *vs.* mCherry/Cre$^{+}$/*Tsc1*$^{-/-}$ 409.6 μm$^2$ ± 9.4; E17: mCherry/*Tsc1*$^{flox/flox}$ 157.3 μm$^2$ ± 3.0 *vs.* mCherry/Cre$^{+}$/*Tsc1*$^{-/-}$ 424.6 μm$^2$ ± 10.2; One-way ANOVA with Bonferroni post-correction ***$p < 0.001$, N = 4–6 mice with 9–33 neurons analyzed per brain slice). There were no morphological differences between neurons of animals IUE at E16 or E17 (see Supplementary Table 1). Electroporation at E18 did not yield any GFP-expressing neurons marking the end of corticogenesis (data not shown). These data indicate that there is a time window spanning several days during embryogenesis rather than a very restricted time point of vulnerability for lack of hamartin to induce dysplastic neurons.

### 3.3. Embryonic loss of Tsc1 leads to abnormal positioning of cortical neurons

Aberrant neuronal morphology or polarity have been suggested to alter migration characteristics of developing, migrating cortical neurons (Falace et al., 2014; LoTurco and Bai, 2006). Our experiments demonstrated altered neuronal morphology upon *Tsc1* knockout in form of substantially increased soma size, which may potentially interfere with neuronal migration or affect their final position within the cortex. In the following set of experiments we ablated *Tsc1* at cortical developmental stages between E14-E18 by *in utero* electroporation of CAG-Cre-GFP and mCherry and analyzed final cortical positioning of electroporated cells at P24-30. Neurons of *Tsc1*$^{flox/flox}$ mice *in utero* electroporated at E14 with control plasmids were mainly located in layer II/III (66.7% ± 8.3) and also in part in upper layer IV (33.3% ± 8.3) whereas *Tsc1* knockout cells were localized in similar amounts in layer II/III (39.7% ± 8.0) and IV (54.4% ± 6.9) and also a few in even lower layers (5.9% ± 2.3) (Fig. 3A, B, G). After IUE at E16 nearly all electroporated control neurons clustered at the upper third of layer II/III (93.4% ± 2.6), *Tsc1* knockout neurons on the other hand were observed to be aberrantly dispersed throughout layers II/III, only 35.2% ± 7.2 neurons were found in the upper half of layer II/III while 50.4% ± 3.9 of the Cre-electroporated neurons were located in the lower layer II/III and 14.4% ± 6.9 in layer IV (Fig. 3C, D, G). Intriguingly, IUE of CAG-Cre-GFP into *Tsc1*$^{flox/flox}$ animals at E17 revealed a more widely dispersion of size increased dysplastic neuronal elements mainly from the middle to the external border of layer II/III, 37.6% ± 8.0 neurons were located in the upper part of layer II/III while 56.7% ± 6.8 neurons were found in lower layer II/III and 5.7% ± 3.5 in layer IV. This

**Fig. 1.** Cre expression in CD1-*Tsc1*$^{flox/flox}$ mice results in increased mTOR pathway activation. CD1-*Tsc1*$^{flox/flox}$ mice were *in utero* electroporated (IUE) at E14 with either CAG-Cre-GFP and mCherry or only mCherry a control. Brain slices of P24-30 mice were afterwards stained with pS6 antibodies. A representative image of the ipsilateral cortex shows strong mCherry and Cre-GFP expression together with high pS6 immunoreactivity (A) in contrast to the contralateral side (B), Scale bar = 100 μm. Cre-electroporated, NeuN-positive neurons appear enlarged and have strong pS6 immunoreactivity (C). In comparison the control (mCherry) electroporated ipsilateral cortex shows mCherry expressing neurons positive for NeuN with low pS6 fluorescence intensity (D), Scale bar = 100 μm. Sholl analysis illustrates the number of intersections of dendrites with circles with increasing distance from the soma (E). *Tsc1* knockout neurons show a significantly increased number of intersections in comparison to control neurons (E), Kolomogorov-Smirnov test: **$p < 0.01$, n = 5 control neurons, n = 8 *Tsc1* knockout neurons). Representative images of single cortical neurons electroporated with CAG-Cre-GFP (F) or mCherry as control (G) used for Sholl analysis, Scale bar = 100 μm. Cre-electroporated *Tsc1* knockout neurons have a larger axon diameter than control neurons (H & I). Scale bar = 25 μm.

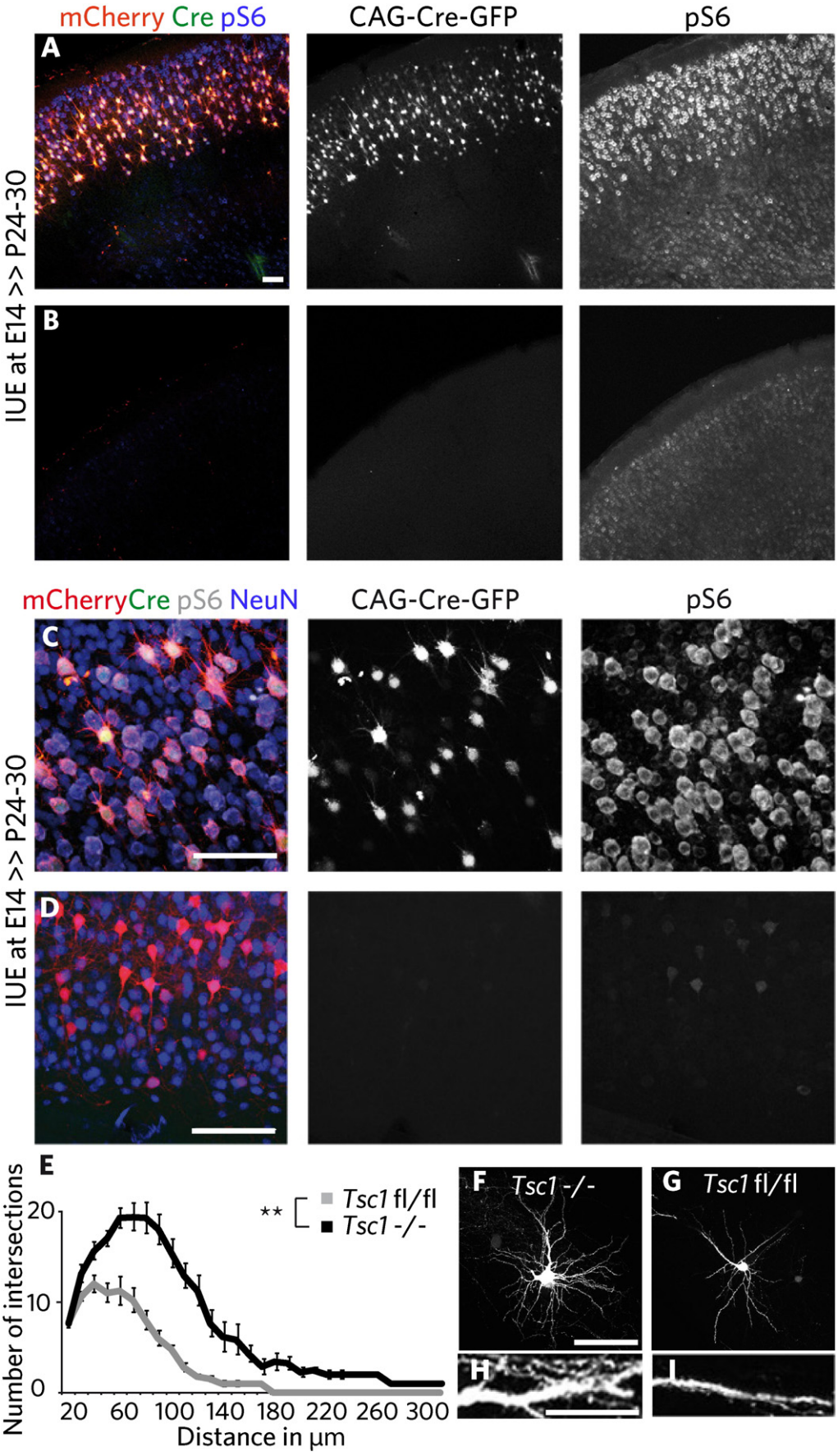
mCherry Cre pS6
CAG-Cre-GFP
pS6
A
B
IUE at E14 >> P24-30
mCherryCre pS6 NeuN
CAG-Cre-GFP
pS6
C
D
IUE at E14 >> P24-30
E
Number of intersections
20
10
0
20 60 100 140 180 220 260 300
Distance in µm
** Tsc1 fl/fl
Tsc1 -/-
F Tsc1 -/-
G Tsc1 fl/fl
H
I

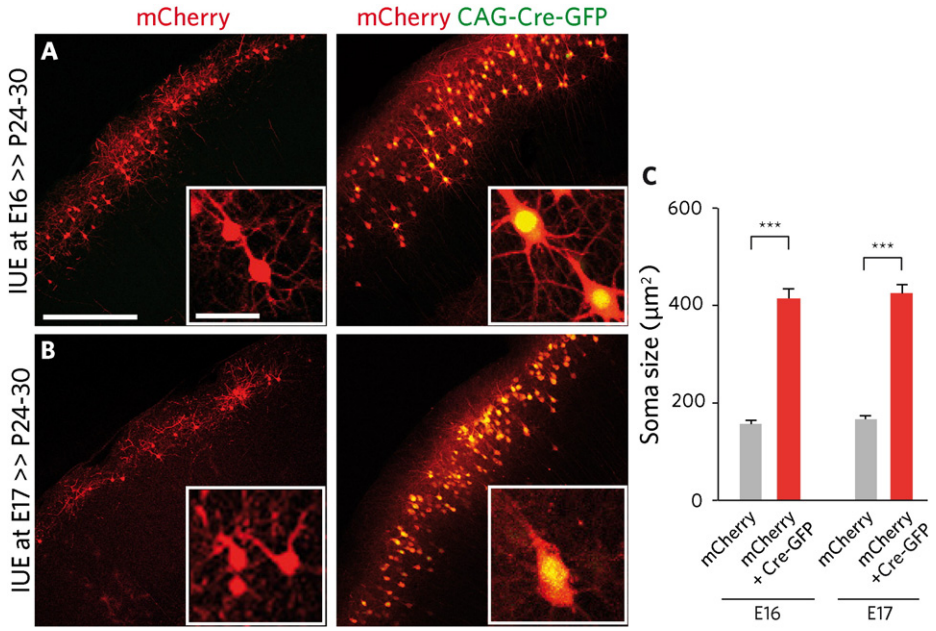


**Fig. 2.** Cre-induced cytological consequences do not depend on the time point of *Tsc1* ablation. *Tsc1*$^{flox/flox}$ mice were *in utero* electroporated (IUE) at different developmental stages with CAG-Cre-GFP and mCherry or only mCherry as control. At P24-30 CAG-Cre-GFP electroporated neurons appear similarly enlarged at E16 (A) and E17 (B) in comparison to controls E16 (A) and E17 (B); Scale bar = 400 μm; Insets show higher magnification images of individual control- or Cre-electroporated cells; Scale bar = 50 μm. Quantification reveals that soma size is more than doubled in CAG-Cre-GFP electroporated neurons and that there is no statistical difference in enhanced soma size between neurons electroporated at E16 and E17 (C). N = 4–6 mice, 3 brain slices per mouse were analyzed; for E16: 22–33 neurons per slice and for E17: 9–23 neurons per slice; One-way ANOVA with Bonferroni post-correction: ***p ≤ 0.001.

was in strong contrast to the normal distribution of neurons electroporated at respective time points with the fluorescent marker only, which formed a very delicate, homogenous band at the external border of layer II (91.6% ± 3.4), as expected when electroporating at such relatively late time points of embryonic development (Fig. 3E, F, G). Again, we did not observe electroporated cells in the cortex, when IUE was carried out at E18 (data not shown).

To further substantiate this analysis we quantified the mean distribution of neurons in the cortex by measuring their distance to layer I (E14: mCherry/*Tsc1*$^{flox/flox}$ 286.2 μm ± 5.8 *vs.* mCherry/Cre$^{+}$/*Tsc1*$^{-/-}$ 413.0 μm ± 4.9; E16: mCherry/*Tsc1*$^{flox/flox}$ 79.5 μm ± 4.0 *vs.* mCherry/Cre$^{+}$/*Tsc1*$^{-/-}$ 245.3 μm ± 5.8; E17: mCherry/*Tsc1*$^{flox/flox}$ 53.5 μm ± 5.8 *vs.* mCherry/Cre$^{+}$/*Tsc1*$^{-/-}$ 116.9 μm ± 6.3; Mann-Whitney *U* test ***p < 0.001, N = 4–11 mice, all neurons on a brain slice were analyzed n = 11–301 cells). This set of experiments indicates that deletion of *Tsc1* during embryonic development dramatically impacts final positioning of cortical neurons and that substantially different neuropathological patterns emerge from the manifestation of *Tsc1* knockout at different time points of embryonic brain development. A comparison of the differential phenotypes caused by control plasmid expression or *Tsc1* knockout at E14, E16 and E17 can be found in Supplementary Table 1.

### 3.4. Differential phenotype rescue requirements for distinct TSC1 allelic variants

We next analyzed, whether the individual *TSC1* variants that were previously observed in cortical tubers as well as in FCD$_{IIb}$ were able to rescue a *Tsc1* knockout *in vivo*. To this end, we co-electroporated CAG-Cre-GFP together with either *TSC1*-WT-2A-mCherry, *TSC1*-H732Y-2A-mCherry, *TSC1*-R692X-2A-mCherry or *TSC1*-R786X-2A-mCherry at E14 and performed the analysis at P24-30 (Fig. 4A–D). Due to the presence of the 2A peptide sequence the *TSC1* variants and the fluorescent marker will be expressed as independent proteins. Intriguingly, our results suggest that the *TSC1*-WT and the *TSC1*-H732Y constructs have the capacity to rescue the *Tsc1*$^{-/-}$ phenotype, at least based on key aspects such as increased soma size and mTOR pathway activation. Neurons expressing Cre and *TSC1*-WT or –H732Y (identified by mCherry labeling) exhibited normal soma size and low pS6 immunoreactivity. In the few neurons that appeared enlarged and also showed increased pS6 immunoreactivity we did not detect *TSC1*-mCherry or Cre-GFP fluorescence (Fig. 4A, B). This may be due to low expression levels of the proteins, which would still result in Cre-mediated recombination and *Tsc1* ablation but no rescue. Neurons could also be solely electroporated with the Cre-GFP plasmid. In contrast, both truncated *TSC1* mutants, *i.e. TSC1*-R692X and *TSC1*-R786X, did not rescue the tuber-like phenotype (Fig. 4C, D). Quantification of the pS6 fluorescence intensity clearly demonstrated a substantially increased pS6 signal (and thus enhanced mTOR activation) in neurons that expressed Cre together with *TSC1*-R692X or *TSC1*-R786X in comparison to neurons that expressed Cre together with *TSC1*-WT or *TSC1*-H732Y. With respect to S6 phosphorylation, these experiments indicate a full rescue capacity of *TSC1*-WT as well as *TSC1*-H732Y since pS6 fluorescence intensity was comparable to cells electroporated with only mCherry (Fig. 1C, quantification Fig. 4E). On the other hand electroporation of *TSC1*-R692X or *TSC1*-R786X led to an increased pS6 fluorescence intensity, comparable to *Tsc1*$^{-/-}$ neurons electroporated with Cre-GFP/mCherry (Fig. 1A, D, quantification Fig. 4E)

**Fig. 3.** Developmental Cre-induced *Tsc1* knockout alters final neuronal position in the cortex. *Tsc1*$^{flox/flox}$ mice were *in utero* electroporated (IUE) with either CAG-Cre-GFP and the volume dye mCherry or only mCherry as control at E14, E16 and E17. Representative images showing brain slices at P24-30 of mice IUE at E14. Approximately 2/3 (66.7%) of the control electroporated neurons are localized in layer II/III (A) where they are evenly distributed and 1/3 (33.3%) in upper layer IV. *Tsc1* knockout neurons on the other hand are more frequently observed in layer IV (54.4%) but also in layer II/III (39.7%) (B). When electroporating at E16 control neurons are mainly located at the upper third of layer II/III (93.4%) (C), whereas Cre-electroporated cells are distributed evenly throughout layer II/III and occasionally a few are found in layer IV (D). At E17 control neurons are clustered around the border of layer II/III and layer I (E) (91.6%) and only a small number of cells is electroporated and expressing the mCherry-tag (25.8 ± 12 cells per 80 μm slice in contrast to >100–300 cells per slice at E14) (A, B, E). *Tsc1* knockout neurons appear widely dispersed all over layer II/III (F), in lower areas of layer II/III (56.7%) but also at upper cortical layer II/III (37.6%). The percentage of neurons in each layer was quantified (G). N = 4–16 mice analyzed, all electroporated neurons in a brain slice were analyzed; for E14: 32–249 neurons per brain slice, E16: 24–301 neurons per slice and for E17: 9–103 neurons per slice; Two-way ANOVA with Bonferroni post-correction and Chi-square test: ***p ≤ 0.001; Scale bar = 400 μm.

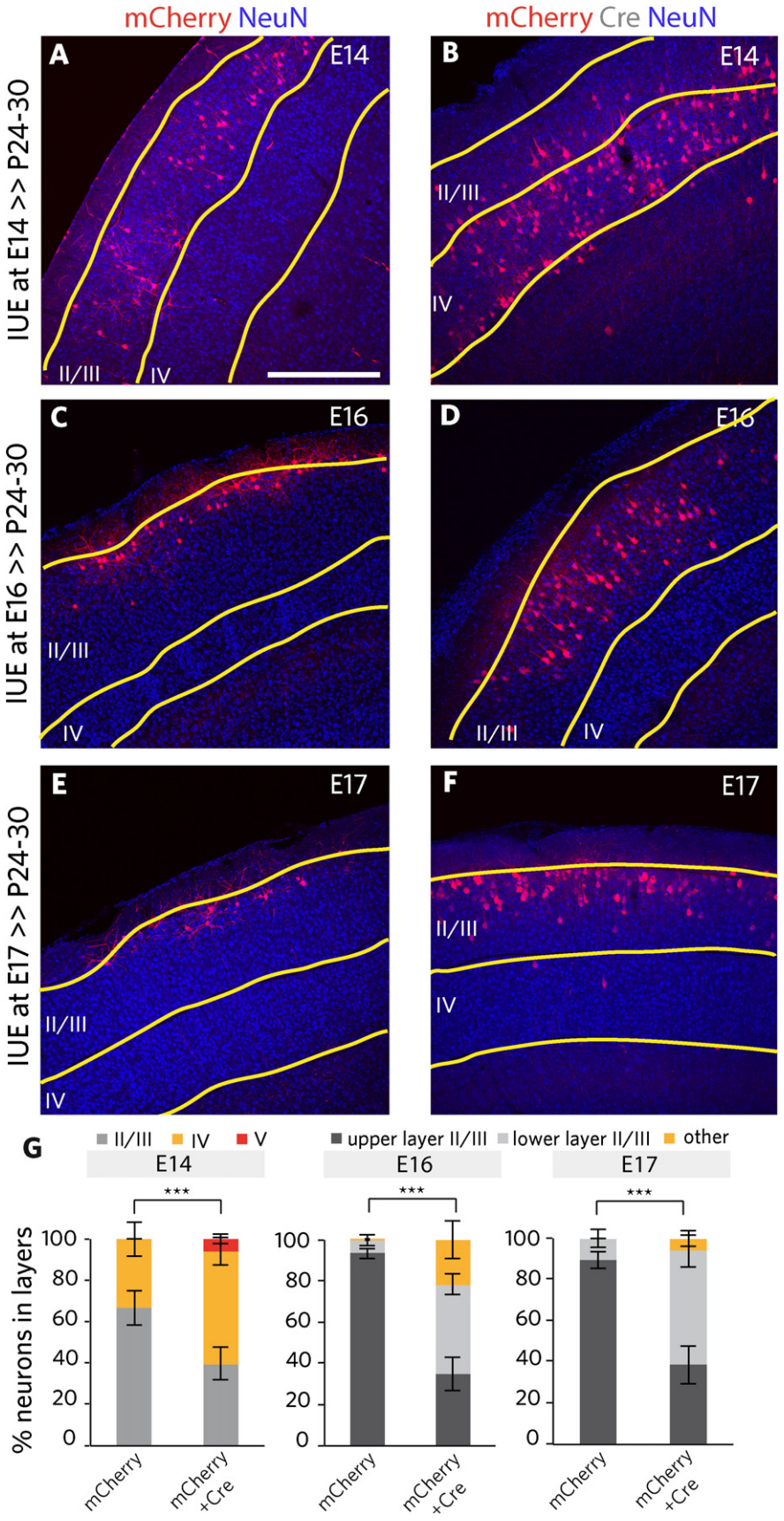
mCherry NeuN
mCherry Cre NeuN
IUE at E14 >> P24-30
IUE at E16 >> P24-30
IUE at E17 >> P24-30
A
E14
II/III
IV
B
E14
II/III
IV
C
E16
II/III
IV
D
E16
II/III
IV
E
E17
II/III
IV
F
E17
II/III
IV
G
II/III
IV
V
upper layer II/III
lower layer II/III
other
E14
E16
E17
***
***
***
% neurons in layers
100
80
60
40
20
0
mCherry
mCherry +Cre

(mCherry/*Tsc1*$^{flox/flox}$ 483.2 a.u. ± 10.6 *vs.* mCherry/Cre$^{+}$/*Tsc1*$^{-/-}$ 1339.5 a.u. ± 39.1, mCherry/Cre$^{+}$/*TSC1*-WT 420.7 a.u. ± 6.4, mCherry/Cre$^{+}$/*TSC1*-H732Y 427.8 a.u. ± 8.7, mCherry/Cre$^{+}$/*TSC1*-R692X 1237.1 a.u. ± 22.0, mCherry/Cre$^{+}$/*TSC1*-R786X 1210.9 a.u. ± 35.7; One-way ANOVA with Bonferroni post-correction ***$p < 0.001$, $N = 6$ mice with 33–41 neurons each).

Corresponding to the activation levels of pS6, the soma sizes were substantially increased in Cre-induced *Tsc1* deficient neurons that were co-expressing either *TSC1*-R692X or *TSC1*-R786X or mCherry alone (*Tsc1*$^{-/-}$) compared to those expressing *TSC1*-WT or *TSC1*-H732Y or neurons without Cre expression (mCherry only) (Fig. 4F) (mCherry/*Tsc1*$^{flox/flox}$ 163.7 μm$^2$ ± 3.0 *vs.* mCherry/Cre$^{+}$/*Tsc1*$^{-/-}$ 391.9 μm$^2$ ± 5.3; mCherry/Cre$^{+}$/*TSC1*-WT 154.8 μm$^2$ ± 3.0, mCherry/Cre$^{+}$/*TSC1*-H732Y 173.0 μm$^2$ ± 2.7, mCherry/Cre$^{+}$/*TSC1*-R692X 431.6 μm$^2$ ± 4.7, mCherry/Cre$^{+}$/*TSC1*-R786X 339.5 μm$^2$ ± 5.9; One-way ANOVA with Bonferroni post-correction ***$p < 0.001$, $N = 6$ mice with 50–65 cells each). These results show that the disease-associated truncated TSC1 variants even if strongly abundant cannot restore normal functionality to *Tsc1*-deficient neurons, whereas the H732Y point mutation in the present setting is as effective as WT-TSC1.

Second hit effects are still rather enigmatic in cortical tubers. Given our present data, we next aimed at elucidating, whether and in which relative concentration *TSC1*-WT was necessary and/or sufficient to rescue the effects of a *TSC1*-stop mutant in a Cre-induced *Tsc1* knockout. To this end we electroporated Cre-GFP at E14 in combination with a mixture of *TSC1*-WT and *TSC1*-R692X, successively decreasing the amount of *TSC1*-WT DNA *versus* the mutant DNA from 10:1 over 1:1 to 1:10 or 1:20. As described above soma size was used as an indicator for mTOR activity. All combinations resulted in the rescue of soma size to control levels (Fig. 5A, B). Only a higher dilution of *TSC1*-WT (1:20) resulted in a slightly, but significantly increased mean soma size (Fig. 5A, B). However, we cannot exclude that single neurons were only electroporated with the more abundant truncated *TSC1* variant (mCherry/*Tsc1*$^{flox/flox}$ 163.7 μm$^2$ ± 3.0; mCherry/Cre$^{+}$/*Tsc1*$^{-/-}$ 391.9 μm$^2$ ± 5.3; mCherry/Cre$^{+}$/*TSC1*-WT:*TSC1*-R692X: 1:1, 171.8 μm$^2$ ± 3.8; 10:1, 167.8 μm$^2$ ± 4.5; 1:10, 162.3 μm$^2$ ± 3.2; 1:20, 280.9 μm$^2$ ± 6.3; One-way ANOVA with Bonferroni post-correction ***$p < 0.001$, $N = 6$–7 mice with 52–65 neurons each). Nevertheless, these data indicate, that even very low TSC1-WT protein levels are entirely sufficient to rescue mTOR hyperactivation and the phenotype of enlarged, dysplastic neurons.

## 4. Discussion

Intraventricular *in utero* electroporation (IUE) represents a tool to scrutinize the effects of gene variants on circumscribed brain areas at controlled time points during development (Chen et al., 2014; LoTurco et al., 2009). Enhanced litter survival can be achieved by using outbreed mouse strains, such as CD1 (Baumgart and Grebe, 2015). Here, we used *Tsc1*$^{flox/flox}$ mice (Kwiatkowski et al., 2002) to induce tuber-like lesions by IUE of a Cre-expressing vector. We observed unexpected, diverging effects of the *TSC1* variants we co-electroporated into *Tsc1* knockout cells. Most importantly, we found that very low concentrations of functional TSC1 protein were sufficient to rescue the cytological phenotype resulting from a complete loss of TSC1, *i.e.* enlargement of cell body and strong pS6 phosphorylation.

We aimed to analyze the effects on neurons and possible implications for tubers of an allelic *TSC1* variant (H732Y), known to be accumulated in frequency in FCD$_{IIb}$ patients (Becker et al., 2002) as well as two truncated versions of TSC1, R692X and R786X, abundant in TSC-associated cortical tubers (Dabora et al., 2001; Hung et al., 2006; Van Slegtenhorst et al., 1999). Previous studies demonstrated that expression of these TSC1 mutant proteins in human embryonic kidney (HEK293T) cells led to reduced binding to tuberin, indicating a functional impairment mediated by hamartin$^{H732Y}$, hamartin$^{R692X}$ and hamartin$^{R786X}$. However, expression of hamartin$^{H732Y}$ *in vivo* did not recapitulate the findings of the cell culture experiments; here we observed a phenotype similar to the *TSC1*-WT rescue with normal-appearing *Tsc1*-knockout neurons indicating at least residual functionality of hamartin$^{H732Y}$. There are several potential explanations for this observation: Firstly, the *in vitro* studies were performed in the non-neuronal (kidney) immortalized, mitotically active tumor cell line HEK293T, which exhibits a distinct proteome, both in composition and posttranslational modifications, and a highly active translational machinery. Thus, different relative expression levels of individual hamartin variants may have been reached in the present *in vivo* and the previous *in vitro* study (Lugnier et al., 2009), low and high, respectively, which may have elicited a phenotype in cell culture experiments not recapitulated here *in vivo*. Alternatively, the expression of the hamartin$^{H732Y}$ variant at time points earlier than E14 may be required to generate a phenotype, however, the experimental strategy limits us to E14-E18. Obviously, the present experiments argue for a rescuing capacity of hamartin$^{H732Y}$ *in vivo* in a cellular background that completely loses the expression of WT hamartin starting at E14. Furthermore, also in the cultured tumor cells the binding of hamartin$^{H732Y}$ to tuberin and their co-localization was not completely abolished but only reduced to 40% and 20%, respectively (Lugnier et al., 2009). In this context, the full rescue potential of *TSC1*-H732Y indicates that the remaining interaction of hamartin$^{H732Y}$ and tuberin in neurons *in vivo* is sufficient for the mutant protein to remain functionally active. Future studies need to be conducted to address this hypothesis and exploit the intriguing possibility that only low levels of TSC1 are sufficient to retain a normal neuronal phenotype which may not be the case for TSC2, possibly providing an explanation for the more severe clinical phenotype observed in TSC patients harboring *TSC2* mutations (Curatolo et al., 2015).

On the other hand, expression of the truncation mutants hamartin$^{R692X}$ as well as hamartin$^{R786X}$ did not rescue the *Tsc1*-knockout phenotype and neurons expressing these hamartin mutants are morphologically similar to *Tsc1* knockout neurons. These findings underline the pathogenic potential of these TSC1 mutants. Despite the morphological alterations induced by *in utero* expression of hamartin$^{R692X}$ we neither observed spontaneous generalized seizures nor differences in Pentylentetrazol-elicited seizures compared to controls in respectively transgenic mice with a C57BL/6 background (data not shown). The absence of spontaneous seizures was also reported in another TSC mouse model of focal *Tsc1* knockout in *Tsc1*$^{fl/mut}$ mice by *in utero* electroporation of CAG-Cre (Feliciano et al., 2011). In fact, various parameters and their complex interplay were demonstrated to profoundly influence the excitability of the lesion: the size and the exact cerebral location of the lesion, the composition of compromised precursor cells and finally, also the age of the individual mouse was recently shown to be critical for seizure occurrence, since mice heterozygous for *Tsc1* lacking tuber-like lesions had spontaneous seizures only until 9–18 days of age (Lozovaya et al., 2014; Jansen et al., 2005; Meikle et al., 2007; Feliciano et al., 2011). Future studies with more sophisticated EEG-analysis set ups

**Fig. 4.** Distinct phenotype rescue requirements for *TSC1* allelic variants. Brain slices of P24-30 *Tsc1*$^{flox/flox}$ mice co-*in utero* electroporated (IUE) with CAG-Cre-GFP and either *TSC1*-WT-2A-mCherry, *TSC1*-H732Y-2A-mCherry, *TSC1*-R692X-2A-mCherry or *TSC1*-R786X-2A-mCherry at E14 were stained against pS6. Representative images show single cells expressing Cre and *TSC1*-WT (A) or *TSC1*-H732Y (B) that appear normal and negative for pS6 and neighboring cells with strong pS6 IR but without *TSC1*-WT expression. Neurons, co-electroporated with CAG-Cre-GFP and *TSC1*-R692X (C) or *TSC1*-R786X (D) appear enlarged with high pS6 fluorescence intensity, even in cells without apparent Cre-expression. Quantification shows significantly increased pS6 fluorescence intensity in *TSC1*-R692X or *TSC1*-R786X electroporated neurons in comparison to *TSC1*-WT or *TSC1*-H732Y electroporated neurons (E). Soma size is significantly elevated in Cre$^{+}$/*TSC1*-R692X and Cre$^{+}$/*TSC1*-R786X electroporated neurons in comparison to Cre$^{+}$/*TSC1*-WT or Cre$^{+}$/*TSC1*-H732Y neurons (F). $N = 6$ mice with 50–65 cells each; One-way ANOVA with Bonferroni post-correction: ***$p \leq 0.001$; Scale bar = 100 μm.

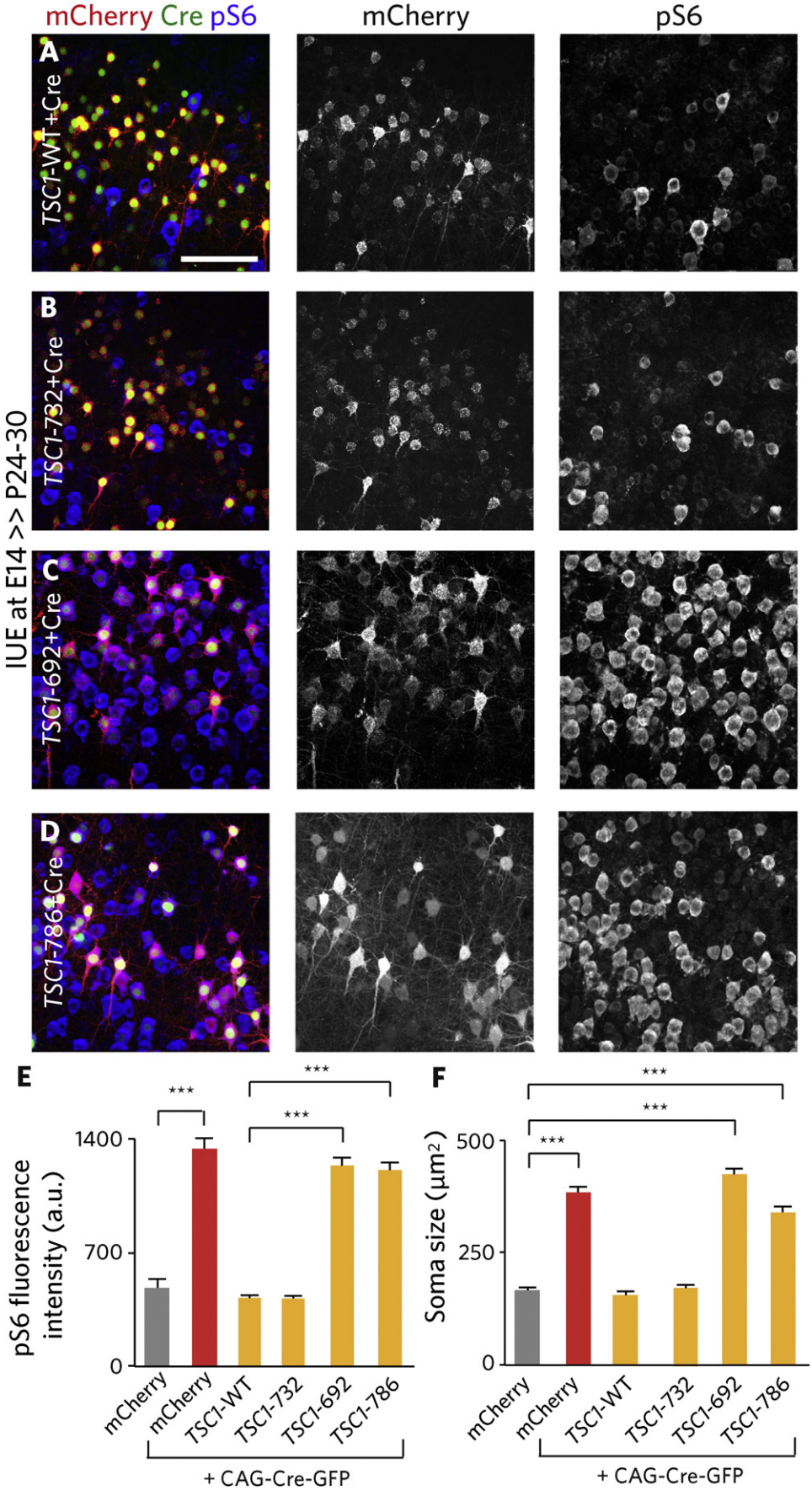
mCherry Cre pS6
mCherry
pS6
A
TSC1-WT+Cre
B
TSC1-732+Cre
C
TSC1-692+Cre
D
TSC1-786+Cre
IUE at E14 >> P24-30
E
pS6 fluorescence intensity (a.u.)
1400
700
0
***
***
***
mCherry
mCherry
TSC1-WT
TSC1-732
TSC1-692
TSC1-786
+ CAG-Cre-GFP
F
Soma size (µm²)
500
250
0
***
***
***
mCherry
mCherry
TSC1-WT
TSC1-732
TSC1-692
TSC1-786
+ CAG-Cre-GFP

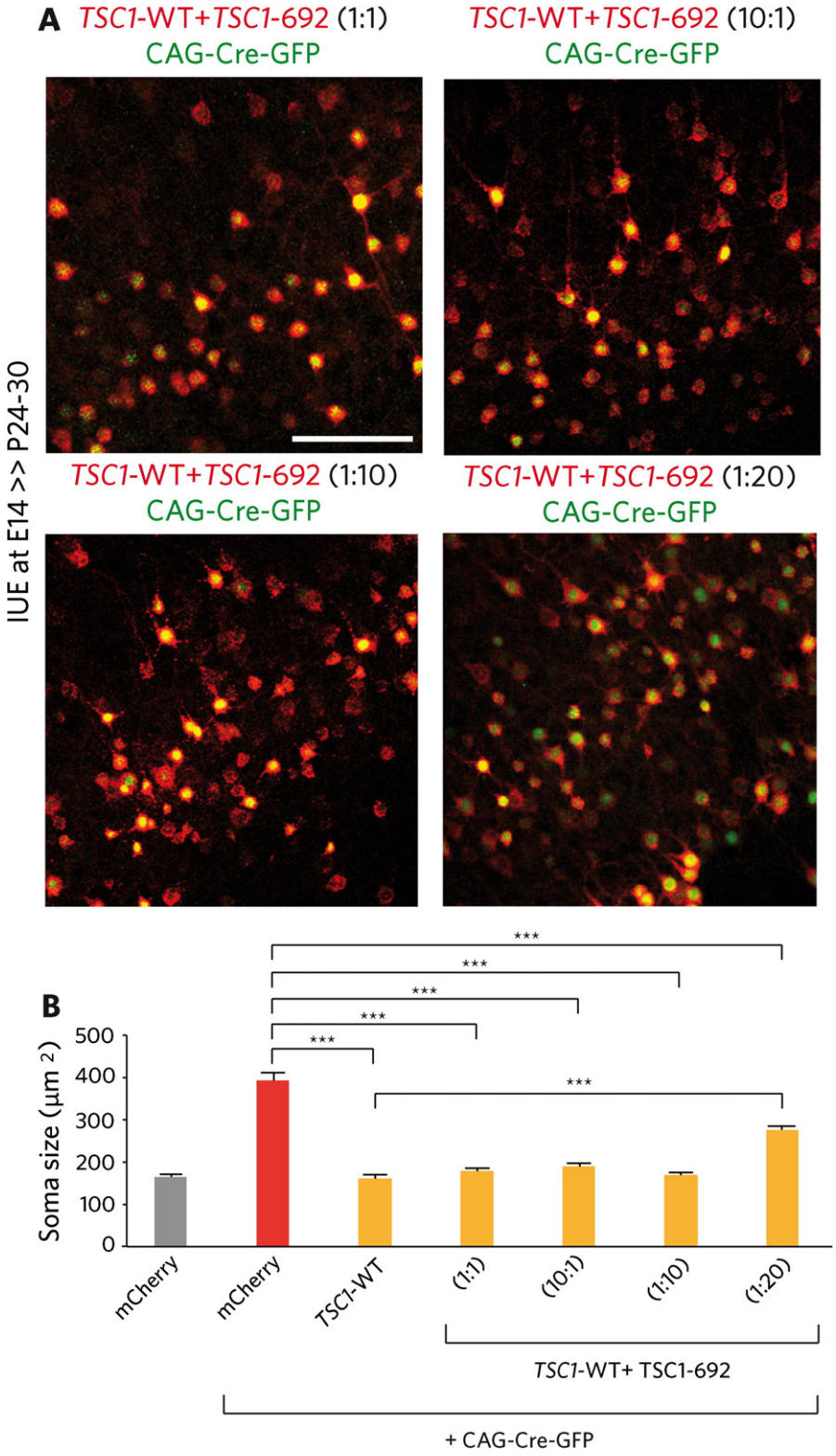


**Fig. 5.** Minimal amounts of wildtype *TSC1* are sufficient to rescue cytological consequences of a *Tsc1* knockout phenotype. *Tsc1*$^{flox/flox}$ mice were *in utero* electroporated (IUE) with CAG-Cre-GFP and different ratios of *TSC1*-WT-2A-mCherry and *TSC1*-R692X-2A-mCherry at E14 and analyzed at P24-30. Soma size appears normal and is similar for the tested ratios, 1:10, 1:1 and 10:1 of *TSC1*-WT-2A-mCherry and *TSC1*-R692X-2A-mCherry (A). Only low relative concentrations of *TSC1*-WT down to 1:20 show a slight increase in soma size (A). Quantification of the mean soma size shows that all tested dilutions have a soma size similar to control-electroporated neurons and are significantly increased in comparison to *Tsc1*-KO neurons (B). However, the 1:20 dilution of *TSC1*-WT is also statistically different from control- and rescue Cre$^{+}$/*TSC1*-WT neurons. N = 6–7 mice with 52–65 neurons each, One-way ANOVA Bonferroni post-correction: ***p ≤ 0.001; Scale bar = 100 µm.

allowing the detection of focal seizures with onset in the lesioned area will be mandatory in order to identify the factors contributing to hyperexcitability in the dysplastic lesions here under study.

In a next set of experiments, we co-electroporated this truncated *TSC1*-R692X mutant with varying amounts of wildtype *TSC1*. Our data revealed, that already small amounts of hamartin-WT were sufficient

for phenotype rescue. This result strongly stresses mechanisms for substantial silencing of the second allele to be extremely critical for the manifestation of cortical tubers. Peripheral TSC-associated tumors such as angiomyolipoma or rhabdomyoma frequently fulfill the so-called '2-hit hypothesis' for inactivation of tumor suppressor genes, *i.e.* mutation of the first and associated LOH of the second allele (Henske et al., 1996; Knudson, 1991, 1996). In contrast, LOH at the *TSC1/TSC2* genomic loci is only occasionally present in cortical tubers (Carbonara et al., 1995; Henske et al., 1996).

Recent data using state-of-the-art deep sequencing in tubers did not reveal a high frequency of second hit mutations of *TSC1* and/or *TSC2* or *KRAS*, an upstream component of the mitogen-activated protein kinase (MAPK) pathway often mutated in cancer (Qin et al., 2010). Obviously, heterozygous germline mutations of *TSC1/TSC2* affect also histologically normal appearing cortex. Circumscribed tubers may therefore require additional yet enigmatic pathogenetic factors for their emergence. Mutations in other components of the mTOR pathway as it was recently shown in hemimegalencephaly (Rivière et al., 2012) as well as in $FCD_{IIb}$ especially with respect to mTOR may be relevant even only in a subset of cells (Lim et al., 2015). On the other hand, hard-to-find intronic mutations, genetic mosaicism of cortical tubers or technology limits may likely account for the cases of TSC with no identified mutations (Curatolo et al., 2015; Tyburczy et al., 2015).

The non-static semiology and episodic emergence of seizures, may argue for molecular alterations affecting hamartin/tuberin to occur on dynamic, *i.e.* epigenetic or protein levels. Recent data demonstrated in smooth muscle-like cells isolated from an angiomyolipoma of a TSC-patient that promoter methylation induces a substantial reduction of tuberin and abnormal developmental effects in respective cells can be successfully antagonized by use of chromatin-remodeling agents (Han et al., 2004; Lesma et al., 2009). It is not resolved, whether parallel mechanisms operate in tubers. Furthermore, post-translational inactivation of tuberin, by non-physiological phosphorylation specific to TSC-associated brain lesions including tubers was attributed to abnormal activation of the Akt and MAPK pathways (Han et al., 2004; Lesma et al., 2009). However, the underlying causes of Akt/MAPK pathway activation remain unclear and may be epigenetically driven. Respective alterations cannot be mimicked or controlled for in the present experimental setup.

Our animal model of TSC partially reproduced the focal abnormal cortical positioning seen in brain biopsies of TSC patients, the so-called cortical tubers as hallmark of TSC. Hamartin loss initiated at E14 led to an increased amount of electroporated, *Tsc1* knockout neurons in layer IV; a layer that can be described as a cortical hub for intracolumnar information processing since it converges the majority of the sensory information (Beierlein et al., 2002; Feldmeyer, 2012). This highly interconnected layer amplifies and redistributes thalamo-cortical inputs and an increased number of layer IV neurons should therefore increase integration and recurrent inputs (Lozovaya et al., 2014). This in turn will foster increased network excitability and hence, contribute to the epileptogenic potential of TSC.

As consequence, the very low levels of wildtype hamartin expression required to rescue the tuber phenotype may provide a promising basis for future gene therapies aiming at reconstituting hamartin expression in tubers. Everolimus has recently proven to be able to reduce the volume and clinical symptoms of TSC-associated subependymal giant cell astrocytomas (Franz et al., 2014), however, this drug may be limited for long-term or even life-long treatment due to substantial side effects. Experimental gene therapy has recently been shown successful in already manifest developmental brain lesions, *i.e.* subcortical band heterotopia and seizures (Manent et al., 2008). Given the relatively minute amounts of wildtype hamartin that are required to rescue the tuber phenotype in our present experiments, gene therapeutic reconstitution of hamartin expression in tubers may be a promising locally restricted strategy that should have substantially less side effects than systemic chronic pharmacotreatment – if any at all. New molecular tools are required for the experimental testing of respective experimental therapies in the future.

## 5. Conclusion

In the present study we used a very recent transgenic mouse model for tuberous sclerosis induced at E14 by *in utero* electroporation reflecting tuber-like neuropathological features such as abnormal positioning of cortical neurons and dramatically enlarged neuronal cell bodies with strong mTOR pathway activation (Carson et al., 2012; Mizuguchi and Takashima, 2001). Cortical tubers are proposed to be the origin of recurrent seizures, however underlying pathogenetic mechanisms leading to their formation remain controversial (Feliciano et al., 2013). With this model we demonstrated that already minute amounts of *TSC1* wildtype were necessary to retain a normal cellular phenotype, arguing in general favor of Knudson's '2-hit hypothesis' as pathogenetic cause for cortical tuber formation. The strong rescuing capacity of functional hamartin should be further analyzed since it indicates a promising basis for gene therapies. With our CD1-*Tsc1*$^{flox/flox}$ mouse model, modified from a recently published mouse model (Feliciano et al., 2011), we obtained substantially increased pup survival, thus facilitating the opportunity to study pathological mechanisms underlying *Tsc1* dysregulation.

Supplementary data to this article can be found online at http://dx.doi.org/10.1016/j.nbd.2016.07.006.

## Conflict of interest statement

The authors declared no conflict of interest.

## Acknowledgement

Our work is supported by Deutsche Forschungsgemeinschaft (SFB1089, BE2078, SCHO820) (AJB, SS), the European Union Seventh Framework Programme (FP7/2007-2013) under grant agreement no 602102 (EPITARGET; AJB, SS), Bundesministerium für Bildung und Forschung (01GQ0806, SS; 01EW1606 - DeCipher EraNet Neuron, AJB), Else Kröner-Fresenius-Stiftung (2010_A145) (AJB, BR, CC), Graduierten-Stipendium der Novartis-Stiftung für Therapeutische Forschung (AG), Fritz Thyssen Stiftung (10.15.2.022MN) (AJB, CC) & the BONFOR program of the University of Bonn Medical Center (O-126.0046, O-154.0114, O-154.0111, O-154.0110, O-154.0108, O-154.0109) (AJB, SS, AG). We thank Sabine Opitz, Lioba Dammer and Daniela Frangenberg for excellent technical assistance. We thank Mark Nellist for providing the *TSC1*-cDNAs and Emilie Pallesi-Pocachard. Particularly, we thank Johannes Schramm, Bonn, for generously supporting our work. Parts of this manuscript contributed to Barbara Robens PhD thesis.

## References

Baumgart, J., Grebe, N., 2015. C57BL/6-specific conditions for efficient in utero electroporation of the central nervous system. J. Neurosci. Methods 240, 116–124.

Baybis, M., Yu, J., Lee, A., Golden, J.A., Weiner, H., McKhann, G., Aronica, E., Crino, P.B., 2004. mTOR cascade activation distinguishes tubers from focal cortical dysplasia. Ann. Neurol. 56, 478–487.

Becker, A.J., Urbach, H., Scheffler, B., Baden, T., Normann, S., Lahl, R., Pannek, H.W., Tuxhorn, I., Elger, C.E., Schramm, J., Wiestler, O.D., Blümcke, I., 2002. Focal cortical dysplasia of Taylor's balloon cell type: mutational analysis of the TSC1 gene indicates a pathogenic relationship to tuberous sclerosis. Ann. Neurol. 52, 29–37.

Beierlein, M., Fall, C.P., Rinzel, J., Yuste, R., 2002. Thalamocortical bursts trigger recurrent activity in neocortical networks: layer 4 as a frequency-dependent gate. J. Neurosci. 22, 9885–9894.

Blümcke, I., Thom, M., Aronica, E., Armstrong, D.D., Vinters, H.V., Palmini, A., Jacques, T.S., Avanzini, G., Barkovich, A.J., Battaglia, G., Becker, A., Cepeda, C., Cendes, F., Colombo, N., Crino, P., Cross, J.H., Delalande, O., Dubeau, F., Duncan, J., Guerrini, R., Kahane, P., Mathern, G., Najm, I., Özkara, Ç., Raybaud, C., Represa, A., Roper, S.N., Salamon, N., Schulze-Bonhage, A., Tassi, L., Vezzani, A., Spreafico, R., 2010. The clinicopathologic spectrum of focal cortical dysplasias: a consensus classification proposed by an ad hoc Task Force of the ILAE Diagnostic Methods Commission. Epilepsia 52, 158–174.

Carbonara, C., Longa, L., Grosso, E., Borrone, C., Garrè, M.G., Brisigotti, M., Migone, N., 1994. 9q34 loss of heterozygosity in a tuberous sclerosis astrocytoma suggests a growth suppressor-like activity also for the TSC1 gene. Hum. Mol. Genet. 3, 1829–1832.
Carbonara, C., Longa, L., Grosso, E., Mazzucco, G., Borrone, C., Garrè, M.L., Brisigotti, M., Filippi, G., Scabar, A., Giannotti, A., Falzoni, P., Monga, G., Garini, G., Gabrielli, M., Riegler, P., Danesino, C., Ruggieri, M., Magro, G., Migone, N., 1995. Apparent preferential loss of heterozygosity at TSC2 over TSC1 chromosomal region in tuberous sclerosis hamartomas. Genes Chromosom. Cancer 15, 18–25.
Carson, R.P., Van Nielen, D.L., Winzenburger, P.A., Ess, K.C., 2012. Neuronal and glia abnormalities in Tsc1-deficient forebrain and partial rescue by rapamycin. Neurobiol. Dis. 45, 369–380.
Chan, J.A., Zhang, H., Roberts, P.S., Jozwiak, S., Wieslawa, G., Lewin-Kowalik, J., Kotulska, K., Kwiatkowski, D.J., 2004. Pathogenesis of tuberous sclerosis subependymal giant cell astrocytomas biallelic inactivation of TSC1 or TSC2 leads to mTOR activation. J. Neuropathol. Exp. Neurol. 63, 1236–1242.
Chen, F., Becker, A.J., LoTurco, J.J., 2014. Contribution of tumor heterogeneity in a new animal model of CNS tumors. Mol. Cancer Res. 12, 742–753.
Cobolli Gigli, C., Scaramuzza, L., Gandaglia, A., Bellini, E., Gabaglio, M., Parolaro, D., Kilstrup-Nielsen, C., Landsberger, N., Bedogni, F., 2016. MeCP2 related studies benefit from the use of CD1 as genetic background. PLoS One 11, e0153473.
Crino, P.B., Aronica, E., Baltuch, G., Nathanson, K.L., 2010. Biallelic TSC gene inactivation in tuberous sclerosis complex. Neurology 74, 1716–1723.
Curatolo, P., Moavero, R., Roberto, D., Graziola, F., 2015. Genotype/phenotype correlations in tuberous sclerosis complex. Semin. Pediatr. Neurol. 22, 259–273.
Dabora, S.L., Jozwiak, S., Franz, D.N., Roberts, P.S., Nieto, A., Chung, J., Choy, Y.-S., Reeve, M.P., Thiele, E., Egelhoff, J.C., Kasprzyk-Obara, J., Domanska-Pakiela, D., Kwiatkowski, D.J., 2001. Mutational analysis in a cohort of 224 tuberous sclerosis patients indicates increased severity of TSC2, compared with TSC1, disease in multiple organs. Am. J. Hum. Genet. 68, 64–80.
Falace, A., Buhler, E., Fadda, M., Watrin, F., Lippiello, P., Pallesi-Pocachard, E., Baldelli, P., Benfenati, F., Zara, F., Represa, A., Fassio, A., Cardoso, C., 2014. TBC1D24 regulates neuronal migration and maturation through modulation of the ARF6-dependent pathway. Proc. Natl. Acad. Sci. U. S. A. 111, 2337–2342.
Feldmeyer, D., 2012. Excitatory neuronal connectivity in the barrel cortex. Front. Neuroanat. 6, 24.
Feliciano, D.M., Su, T., Lopez, J., Platel, J.-C., Bordey, A., 2011. Single-cell Tsc1 knockout during corticogenesis generates tuber-like lesions and reduces seizure threshold in mice. J. Clin. Invest. 121, 1596–1607.
Feliciano, D.M., Lin, T.V., Hartman, N.W., Bartley, C.M., Kubera, C., Hsieh, L., Lafourcade, C., O'Keefe, R.A., Bordey, A., 2013. A circuitry and biochemical basis for tuberous sclerosis symptoms: from epilepsy to neurocognitive deficits. Int. J. Dev. Neurosci. 31, 667–678.
Franz, D.N., Belousova, E., Sparagana, S., Bebin, E.M., Frost, M., Kuperman, R., Witt, O., Kohrman, M.H., Flamini, J.R., Wu, J.Y., Curatolo, P., de Vries, P.J., Berkowitz, N., Anak, O., Niolat, J., Jozwiak, S., 2014. Everolimus for subependymal giant cell astrocytoma in patients with tuberous sclerosis complex: 2-year open-label extension of the randomised EXIST-1 study. Lancet Oncol. 15, 1513–1520.
Gomez, M.R., 1988. Varieties of expression of tuberous sclerosis. Neurofibromatosis 1, 330–338.
Green, A.J., Johnson, P.H., Yates, J., 1994. The tuberous sclerosis gene on chromosome 9q34 acts as a growth suppressor. Hum. Mol. Genet. 3, 1833–1834.
Grote, A., Robens, B.K., Blümcke, I., Becker, A.J., Schoch, S., Gembe, E., 2016. LRP12 silencing during brain development results in cortical dyslamination and seizure sensitization. Neurobiol. Dis. 86, 170–176.
Han, S., Santos, T.M., Puga, A., Roy, J., Thiele, E.A., McCollin, M., Stemmer-Rachamimov, A., Ramesh, V., 2004. Phosphorylation of tuberin as a novel mechanism for somatic inactivation of the tuberous sclerosis complex proteins in brain lesions. Cancer Res. 64, 812–816.
Hengstschläger, M., Rodman, D.M., Miloloza, A., Hengstschläger-Ottnad, E., Rosner, M., Kubista, M., 2001. Tuberous sclerosis gene products in proliferation control. Mutat. Res. 488, 233–239.
Henske, E.P., Scheithauer, B.W., Short, M.P., Wollmann, R., Nahmias, J., Hornigold, N., Van Slegtenhorst, M., Welsh, C.T., Kwiatkowski, D.J., 1996. Allelic loss is frequent in tuberous sclerosis kidney lesions but rare in brain lesions. Am. J. Hum. Genet. 59, 400–406.
Henske, E.P., Wessner, L.L., Golden, J., Scheithauer, B.W., Vortmeyer, A.O., Zhuang, Z., Klein-Szanto, A., Kwiatkowski, D.J., Yeung, R.S., 1997. Loss of tuberin in both subependymal giant cell astrocytomas and angiomyolipomas supports a two-hit model for the pathogenesis of tuberous sclerosis tumors. Am. J. Pathol. 151, 1639–1647.
Hung, C.-C., Su, Y.-N., Chien, S.-C., Liou, H.-H., Chen, C.-C., Chen, P.-C., Hsieh, C.-J., Chen, C.-P., Lee, W.-T., Lin, W.-L., Lee, C.-N., 2006. Molecular and clinical analyses of 84 patients with tuberous sclerosis complex. BMC Med. Genet. 7, 72.
Jansen, L.A., Uhlmann, E.J., Crino, P.B., Gutmann, D.H., Wong, M., 2005. Epileptogenesis and reduced inward rectifier potassium current in tuberous sclerosis complex-1-deficient astrocytes. Epilepsia 46, 1871–1880.
Knudson, A.G., 1991. Overview: genes that predispose to cancer. Mutat. Res. 247, 185–190.
Knudson, A.G., 1996. Hereditary cancer: two hits revisited. J. Cancer Res. Clin. Oncol. 122, 135–140.
Kwiatkowski, D.J., Zhang, H., Bandura, J.L., Heiberger, K.M., Glogauer, M., el-Hashemite, N., Onda, H., 2002. A mouse model of TSC1 reveals sex-dependent lethality from liver hemangiomas, and up-regulation of p70S6 kinase activity in Tsc1 null cells. Hum. Mol. Genet. 11, 525–534.
Lesma, E., Sirchia, S.M., Ancona, S., Carelli, S., 2009. The methylation of the TSC2 promoter underlies the abnormal growth of TSC2 angiomyolipoma-derived smooth muscle cells. Am. J. Pathol. 174, 2150–2159.
Lim, J.S., Kim, W.-I., Kang, H.-C., Kim, S.H., Park, A.H., Park, E.K., Cho, Y.-W., Kim, S., Kim, H.M., Kim, J.A., Kim, J., Rhee, H., Kang, S.-G., Kim, H.D., Kim, D., Kim, D.-S., Lee, J.H., 2015. Brain somatic mutations in mTor cause focal cortical dysplasia type II leading to intractable epilepsy. Nat. Med. 21, 395–400.
Taylor, D.C., Falconer, M.A., Bruton, C.J., Corsellis, J.A., 1971. Focal dysplasia of the cerebral cortex in epilepsy. J. Neurol. Neurosurg. Psychiatr. 34, 369–387.
LoTurco, J.J., Bai, J., 2006. The multipolar stage and disruptions in neuronal migration. Trends Neurosci. 29, 407–413.
LoTurco, J., Manent, J.B., Sidiqi, F., 2009. New and improved tools for in utero electroporation studies of developing cerebral cortex. Cereb. Cortex 19, i120–i125.
Lozovaya, N., Gataullina, S., Tsintsadze, T., Tsintsadze, V., Pallesi-Pocachard, E., Minlebaev, M., Goriounova, N.A., Buhler, E., Watrin, F., Shityakov, S., Becker, A.J., Bordey, A., Milh, M., Scavarda, D., Bulteau, C., Dorfmuller, G., Delalande, O., Represa, A., Cardoso, C., Dulac, O., Ben-Ari, Y., Burnashev, N., 2014. Selective suppression of excessive GluN2C expression rescues early epilepsy in a tuberous sclerosis murine model. Nat. Commun. 5, 1–15.
Lugnier, C., Majores, M., Fassunke, J., Pernhorst, K., Niehusmann, P., Simon, M., Nellist, M., Schoch, S., Becker, A., 2009. Hamartin variants that are frequent in focal dysplasias and cortical tubers have reduced tuberin binding and aberrant subcellular distribution in vitro. J. Neuropathol. Exp. Neurol. 68, 1136–1146.
Manent, J.-B., Wang, Y., Chang, Y., Paramasivam, M., LoTurco, J.J., 2008. Dcx reexpression reduces subcortical band heterotopia and seizure threshold in an animal model of neuronal migration disorder. Nat. Med. 15, 84–90.
Meikle, L., Talos, D.M., Onda, H., Pollizzi, K., Rotenberg, A., Sahin, M., Jensen, F.E., Kwiatkowski, D.J., 2007. A mouse model of tuberous sclerosis: neuronal loss of Tsc1 causes dysplastic and ectopic neurons, reduced myelination, seizure activity, and limited survival. J. Neurosci. 27, 5546–5558.
Mizuguchi, M., Takashima, S., 2001. Neuropathology of tuberous sclerosis. Brain Dev. 23, 508–515.
Piedimonte, L.R., Wailes, I.K., Weiner, H.L., 2006. Tuberous sclerosis complex: molecular pathogenesis and animal models. Neurosurg. Focus. 20, E4.
Qin, W., Chan, J.A., Vinters, H.V., Mathern, G.W., Franz, D.N., Taillon, B.E., Bouffard, P., Kwiatkowski, D.J., 2010. Analysis of TSC cortical tubers by deep sequencing of TSC1, TSC2 and KRAS demonstrates that small second-hit mutations in these genes are rare events. Brain Pathol. 20, 1096–1105.
Ristanović, D., Milošević, N.T., Štulić, V., 2006. Application of modified sholl analysis to neuronal dendritic arborization of the cat spinal cord. J. Neurosci. Methods 158, 212–218.
Rivière, J.-B., Mirzaa, G.M., O'Roak, B.J., Beddaoui, M., Alcantara, D., Conway, R.L., St-Onge, J., Schwartzentruber, J.A., Gripp, K.W., Nikkel, S.M., Worthylake, T., Sullivan, C.T., Ward, T.R., Butler, H.E., Kramer, N.A., Albrecht, B., Armour, C.M., Armstrong, L., Caluseriu, O., Cytrynbaum, C., Drolet, B.A., Innes, A.M., Lauzon, J.L., Lin, A.E., Mancini, G.M.S., Meschino, W.S., Reggin, J.D., Saggar, A.K., Lerman-Sagie, T., Uyanik, G., Weksberg, R., Zirn, B., Beaulieu, C.L., Majewski, J., Bulman, D.E., O'Driscoll, M., Shendure, J., Graham, J.M., Boycott, K.M., Dobyns, W.B., 2012. De novo germline and postzygotic mutations in AKT3, PIK3R2 and PIK3CA cause a spectrum of related megalencephaly syndromes. Nat. Genet. 44, 934–940.
Saito, T., 2006. In vivo electroporation in the embryonic mouse central nervous system. Nat. Protoc. 1, 1552–1558.
Sampson, J.R., Harris, P.C., 1994. The molecular genetics of tuberous sclerosis. Hum. Mol. Genet. 3, 1477–1480.
Scheidenhelm, D.K., Gutmann, D.H., 2004. Mouse models of tuberous sclerosis complex. J. Child Neurol. 19, 726–733.
Sholl, D.A., 1953. Dendritic organization in the neurons of the visual and motor cortices of the cat. J. Anat. 87, 387–406.
Tavazoie, S.F., Alvarez, V.A., Ridenour, D.A., Kwiatkowski, D.J., Sabatini, B.L., 2005. Regulation of neuronal morphology and function by the tumor suppressors Tsc1 and Tsc2. Nat. Neurosci. 8, 1727–1734.
Tyburczy, M.E., Dies, K.A., Glass, J., Camposano, S., Chekaluk, Y., Thorner, A.R., Lin, L., Krueger, D., Franz, D.N., Thiele, E.A., Sahin, M., Kwiatkowski, D.J., 2015. Mosaic and intronic mutations in TSC1/TSC2 explain the majority of TSC patients with no mutation identified by conventional testing. PLoS Genet. 11, e1005637.
Uhlmann, E.J., Apicelli, A.J., Baldwin, R.L., Burke, S.P., Bajenaru, M.L., Onda, H., Kwiatkowski, D., Gutmann, D.H., 2002. Heterozygosity for the tuberous sclerosis complex (TSC) gene products results in increased astrocyte numbers and decreased p27-Kip1 expression in TSC2+/− cells. Oncogene 21, 4050–4059.
Van Slegtenhorst, M.V., de Hoogt, R., Hermans, C., Nellist, M., Janssen, B., Verhoef, S., Lindhout, D., van den Ouweland, A., Halley, D., Young, J., Burley, M., Jeremiah, S., Woodward, K., Nahmias, J., Fox, M., Ekong, R., Osborne, J., Wolfe, J., Povey, S., Snell, R.G., Cheadle, J.P., Jones, A.C., Tachataki, M., Ravine, D., Sampson, J.R., Reeve, M.P., Richardson, P., Wilmer, F., Munro, C., Hawkins, T.L., Sepp, T., Ali, J.B., Ward, S., Green, A.J., Yates, J.R., Kwiatkowska, J., Henske, E.P., Short, M.P., Haines, J.H., Jozwiak, S., Kwiatkowski, D.J., 1997. Identification of the tuberous sclerosis gene TSC1 on chromosome 9q34. Science 277, 805–808.
Van Slegtenhorst, M., Nellist, M., Nagelkerken, B., Cheadle, J., Snell, R., van den Ouweland, A., Reuser, A., Sampson, J., Halley, D., van der Sluijs, P., 1998. Interaction between hamartin and tuberin, the TSC1 and TSC2 gene products. Hum. Mol. Genet. 7, 1053–1057.
Van Slegtenhorst, M., Verhoef, S., Tempelaars, A., Bakker, L., Wang, Q., Wessels, M., Bakker, R., Nellist, M., Lindhout, D., Halley, D., van den Ouweland, A., 1999. Mutational spectrum of the TSC1 gene in a cohort of 225 tuberous sclerosis complex patients: no evidence for genotype-phenotype correlation. J. Med. Genet. 36, 285–289.